Eur. Phys. J. C (2018) 78:1018
https://doi.org/10.1140/epjc/s10052-018-6495-4

THE EUROPEAN PHYSICAL JOURNAL C

Regular Article - Theoretical Physics

Some hadronic parameters of charmonia in $N_f = 2$ lattice QCD

Gabriela Bailas[1], **Benoît Blossier**[2,a], **Vincent Morénas**[1]

[1] Laboratoire de Physique de Clermont, Unité Mixte de Recherche 6533 CNRS/IN2P3, Université Blaise Pasclal, 4 Avenue Blaise Pascal, TSA 60026, 63171 Aubière Cedex, France
[2] Laboratoire de Physique Théorique, Unité Mixte de Recherche 8627 du Centre National de la Recherche Scientifique, CNRS, Univ. Paris-Sud et Université Paris-Saclay, Bâtiment 210, 91405 Orsay Cedex, France

Received: 5 June 2018 / Accepted: 24 November 2018 / Published online: 15 December 2018

Abstract The phenomenology of leptonic decays of quarkonia holds many interesting features: for instance, it can establish constraints on scenarios beyond the Standard Model with the Higgs sector enriched by a light CP-odd state. In the following paper, we report on a two-flavor lattice QCD study of the η_c and J/ψ decay constants, $f_{\eta_c} = 387(3)(3)$ MeV and $f_{J/\psi} = 399(4)(2)$ MeV. We also examine some properties of the first radial excitation $\eta_c(2S)$ and $\psi(2S)$.

1 Introduction

The discovery at LHC of the Higgs boson with a mass of 125.09(24) GeV [1] has been a major milestone in the history of Standard Model (SM) tests: the spontaneous breaking of electroweak symmetry generates masses of charged leptons, quarks and weak bosons. A well-known issue with the SM Higgs is that the quartic term in the Higgs Lagrangian induces for the Higgs mass m_H a quadratic divergence with the hard scale of the theory: it is related to the so-called hierarchy problem. Several scenarios beyond the SM are proposed to fix that theoretical caveat. Minimal extensions of the Higgs sector contain two complex scalar isodoublets $\Phi_{1,2}$ which, after the spontaneous breaking of the electroweak symmetry, lead to 2 charged particles $H^{\pm}$, 2 CP-even particles h (SM-like Higgs) and H, and 1 CP-odd particle A. In that class of scenarios, quarks are coupled to the CP-odd Higgs through a pseudoscalar current. Those extensions of the Higgs sector have interesting phenomenological implications, especially as far as pseudoscalar quarkonia are concerned. For example, their leptonic decay is highly suppressed in the SM because it occurs *via* quantum loops but it can be reinforced by the new tree-level contribution involving the CP-odd Higgs boson, in particular in the region of parameter space where the new boson is light ($10\,\text{GeV} \lesssim m_A \lesssim 100\,\text{GeV}$) and where the ratio of vacuum expectation values $\tan\beta$ is small ($\tan\beta < 10$) [2,3]. Any enhanced observation with respect to the SM expectation would be indeed a clear signal of New Physics. Let us finally note that the hadronic inputs, which constrain the CP-odd Higgs coupling to heavy quarks through processes involving quarkonia, are the decay constants f_{η_c} and f_{η_b}.

This paper reports an estimate of hadronic parameters in the charmonia sector using lattice QCD with $N_f = 2$ dynamical quarks: namely, the pseudoscalar decay constant f_{η_c}, because of its phenomenological importance, but also the vector decay constant $f_{J/\psi}$ as well as the ratio of masses $m_{\eta_c(2S)}/m_{\eta_c}$ and $m_{\psi(2S)}/m_{J/\psi}$. The two latter quantities are very well measured by experiments and their estimation has helped us to understand how much our analysis method can address the systematic effects, on quarkonia physics, coming from the lattice ensembles we have considered. We present also our findings for the following ratios of decay constants: $f_{\eta_c(2S)}/f_{\eta_c}$ and $f_{\psi(2S)}/f_{J/\psi}$.

This work is an intermediary step before going to the bottom sector, the final target of our program, because it is more promising for the phenomenology of extended Higgs sectors. An extensive study of the spectoscopy of charmonia has been done in [4,5] while only two lattice estimates of f_{η_c} and $f_{J/\psi}$ are available so far at $N_f = 2$ [6] and $N_f = 2 + 1$ [7,8].

2 Lattice computation

2.1 Lattice set-up

This study has been performed using a subset of the CLS ensembles. These ensembles were generated with $N_f = 2$ nonperturbatively $\mathcal{O}(a)$-improved Wilson-Clover fermions [9,10] and the plaquette gauge action [11] for gluon fields, by using either the DD-HMC algorithm [12–15] or the

[a] e-mail: benoit.blossier@th.u-psud.fr

Table 1 Parameters of the simulations: bare coupling $\beta = 6/g_0^2$, lattice resolution, hopping parameter κ, lattice spacing a in physical units, pion mass, number of gauge configurations and bare charm quark masses

id	β	$(L/a)^3 \times (T/a)$	κ_{sea}	a (fm)	m_π (MeV)	Lm_π	# cfgs	κ_c
E5	5.3	$32^3 \times 64$	0.13625	0.065	440	4.7	200	0.12724
F6		$48^3 \times 96$	0.13635		310	5	120	0.12713
F7		$48^3 \times 96$	0.13638		270	4.3	200	0.12713
G8		$64^3 \times 128$	0.13642		190	4.1	176	0.12710
N6	5.5	$48^3 \times 96$	0.13667	0.048	340	4	192	0.13026
O7		$64^3 \times 128$	0.13671		270	4.2	160	0.13022

MP-HMC algorithm [16]. We collect in Table 1 our simulation parameters. Two lattice spacings $a_{\beta=5.5} = 0.04831(38)$ fm and $a_{\beta=5.3} = 0.06531(60)$ fm, resulting from a fit in the chiral sector [17], are considered. We have taken simulations with pion masses in the range [190 , 440] MeV. The charm quark mass has been tuned after a linear interpolation of $m^2_{D_s}$ in $1/\kappa_c$ at its physical value [18], after the fixing of the strange quark mass [19]. The statistical error on raw data is estimated from the jackknife procedure: two successive measurements are sufficiently separated in trajectories along the Monte-Carlo history to neglect autocorrelation effects. Moreover, statistical errors on quantities extrapolated at the physical point are computed as follows. Inspired by the bootstrap prescription, we perform a large set of N_{event} fits of vectors of data whose dimension is the number of CLS ensembles used in our analysis (i.e. $n = 6$) and where each component i of those vectors is filled with an element randomly chosen among the $N_{\text{bins}}(i)$ binned data per ensemble. The variance over the distribution of those N_{event} fit results, obtained with such "random" inputs, is then an estimator of the final statistical error. Finally, we have computed quark propagators through two-point correlation functions using stochastic sources which are different from zero in a single timeslice that changes randomly for each measurement. We have also applied spin dilution and the one-end trick to reduce the stochastic noise [20,21]. In our study we have neglected any contribution from disconnected diagrams.

2.1.1 GEVP discussion

The two-point correlation functions under investigation read

$$C_{\Gamma\Gamma'}(t) = \frac{1}{V}\sum_{\vec{x},\vec{y}} \langle \left[\bar{c}\,\Gamma c\right](\vec{y},t)\left[\bar{c}\,\gamma_0\,\Gamma'\gamma_0\,c\right](\vec{x},0)\,\rangle \qquad (1)$$

where V is the spatial volume of the lattice, $\langle\cdots\rangle$ is the expectation value over gauge configurations, and the interpolating fields $\bar{c}\Gamma c$ can be non-local. As a preparatory work, different possibilities were explored to find the best basis of operators, combining levels of Gaussian smearing, interpolating fields with a covariant derivative $\bar{c}\Gamma(\vec{\gamma}\cdot\vec{\nabla})c$ and operators that are odd under time parity. Solving the Generalized Eigenvalue Problem (GEVP) [22,23] is a key point in this analysis. Looking at the literature we have noticed that people tried to mix together the operators $\bar{c}\Gamma c$ and $\bar{c}\gamma_0\Gamma c$ in a unique GEVP system [4,6]. In our point of view, this approach raises some questions: let us take the example of the interpolating fields $\{P = \bar{c}\gamma_5 c\,;\ A_0 = \bar{c}\gamma_0\gamma_5 c\}$. The asymptotic behaviours of the 2-pt correlation functions defined with these interpolating fields read

$$\begin{cases} \langle P(t)\,P(0)\,\rangle\,;\ \langle A_0(t)\,A_0(0)\,\rangle \xrightarrow{t\to\infty} \cosh[m_P(T/2-t)] \\ \langle P(t)\,A_0(0)\,\rangle\,;\ \langle A_0(t)\,P(0)\,\rangle \xrightarrow{t\to\infty} \sinh[m_P(T/2-t)] \end{cases}$$

The matrix of 2×2 correlators of the GEVP is then

$$C(t) = \begin{bmatrix} \langle P(t)\,P(0)\,\rangle & \langle A_0(t)\,P(0)\,\rangle \\ \langle P(t)\,A_0(0)\,\rangle & \langle A_0(t)\,A_0(0)\,\rangle \end{bmatrix}$$
$$\text{GEVP}: C(t)\,v_n(t,t_0) = \lambda_n(t,t_0)\,C(t_0)\,v_n(t,t_0).$$

In the general case, the spectral decomposition of $C_{ij}(t)$ is

$$C_{ij}(t) = \sum_n Z_n^i Z_n^{*j}[D_{ij}\rho_n^{(1)}(t) + (1-D_{ij})\rho_n^{(2)}(t)]$$
$$\text{where}\quad D_{ij} = 0 \text{ or } 1$$

and with

$$\rho^{(1),(2)}(t) \sim e^{-m_P t}\cosh[m_P(T/2-t)]$$
$$\text{or}\quad e^{-m_P t}\sinh[m_P(T/2-t)]$$

The dual vector u_n to $Z's$ is defined by

$$\sum_j Z_m^{*j} u_n^j = \delta_{mn}$$

Inserted in the GEVP, it gives

$$\begin{aligned}\sum_j C_{ij}(t)u_n^j &= \sum_{j,m} Z_m^i Z_m^{*j} u_n^j\left[D_{ij}\rho_m^{(1)}(t) + (1-D_{ij})\rho_m^{(2)}(t)\right] \\ &= \sum_m \rho_m^{(2)}(t) Z_m^i \sum_j Z_m^{*j} u_n^j \\ &\quad + \sum_m \left(\rho_m^{(1)}(t) - \rho_m^{(2)}(t)\right) Z_m^i \sum_j D_{ij} Z_m^{*j} u_n^j \\ &= \rho_n^{(2)}(t) Z_n^i + \sum_m \left(\rho_m^{(1)}(t)\right. \\ &\quad \left. -\rho_m^{(2)}(t)\right) Z_m^i \sum_j D_{ij} Z_m^{*j} u_n^j\end{aligned}$$

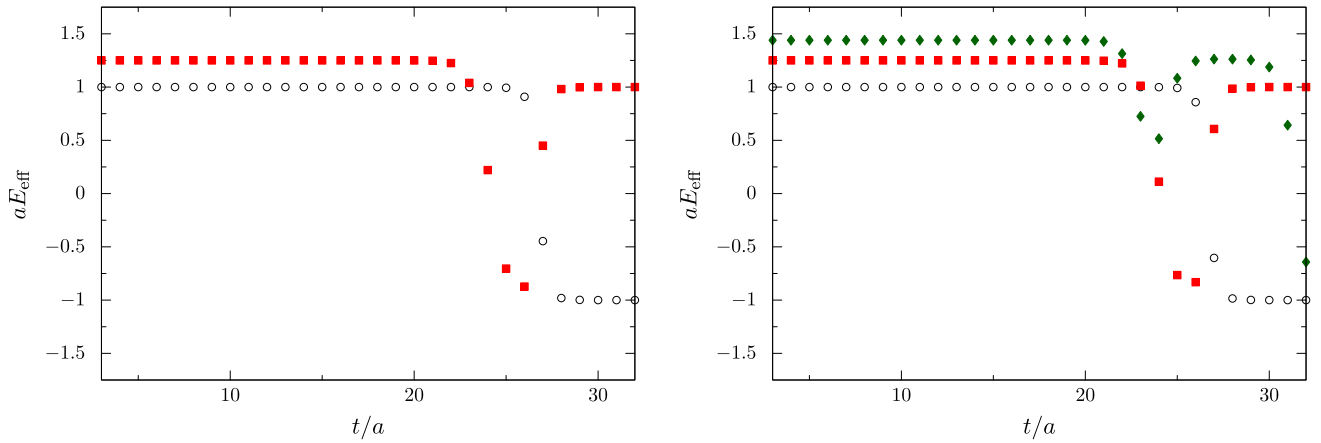

Fig. 1 Effective masses obtained from the 2×2 subsystem (left panel) and the 3×3 subsystem (right panel) of our toy model, with $T = 64$ and $t_0 = 3$

If D_{ij} is independent of i, j, we can write

$$C(t)u_n = \rho(t)Z_n \quad \text{and} \quad \lambda_n(t,t_0) = \frac{\rho_n(t)}{\rho_n(t_0)}$$

However, in the case of mixing T-odd and T-even operators in a single GEVP, the D's *do depend* on i and j: the previous formula for $\lambda_n(t,t_0)$ is then not correct. Hence, approximating every correlator by sums of exponentials forward in time, together with the assumption that the D_{ij} are independent of i and j, may face caveats. A toy model with 3 states in the spectrum helps to understand this issue:

spectrum
1.0
1.25
1.44

Matrix of couplings

$$\begin{bmatrix} 0.6 & 0.25 & 0.08 \\ 0.61 & 0.27 & 0.08 \\ 0.58 & 0.24 & 0.08 \end{bmatrix}$$

time behaviour of C_{ij}

$$\begin{bmatrix} \cosh & \sinh & \cosh \\ \sinh & \cosh & \sinh \\ \cosh & \sinh & \cosh \end{bmatrix}$$

The effective energy $E^{\rm eff}$ obtained by solving the GEVP writes

$$aE_n^{\rm eff} = \ln\left(\frac{\lambda_n(t,t_0)}{\lambda_n(t+a,t_0)}\right)$$

In our numerical application, we have chosen $T = 64, t_0 = 3$ and compared 2×2 and 3×3 subsystems: results can be seen in Fig. 1. Our observation is that until $t = T/4$, neglecting the time-backward contribution in the correlation function has no effect. Based on this study, we can affirm that the method is safe for the ground state and the first excitation. In contrast, one may wonder what would happen with a dense spectrum when the energy of the third or a higher excited state is extracted: in that case there will be a competition between the contamination from higher states, which are not properly isolated by the finite GEVP system, and the omission of the backward in time contribution to the generalised eigenvalue under study, even at times $t < 1$ fm.

2.1.2 *Interpolating field basis*

Building a basis of operators with

$$\left\{\bar{c}\,\Gamma c\,;\ \bar{c}\,\Gamma(\vec{\gamma}\cdot\vec{\nabla})c\right\} \quad \text{where}$$

$$\nabla_\mu\psi(x) = \frac{U_\mu(x)\psi(x+a\hat{\mu}) - U_\mu^\dagger(x-a\hat{\mu})\psi(x-a\hat{\mu})}{2a}$$

can have advantages and this was already explored [24,25]. But there are sometimes bad surprises…a good example being the pseudoscalar-pseudoscalar correlator defined by

$$C(t) \;=\; \langle\left[\bar{c}\,\gamma^5(\vec{\gamma}\cdot\vec{\nabla})c\right](t)\left[\bar{c}\,\gamma^5(\vec{\gamma}\cdot\vec{\nabla})c\right](0)\,\rangle$$

whose behaviour will be anticipated using the quark model method.
In the formalism of quark models, the c quark field reads

$$c(\vec{p}_c) \;=\; \begin{pmatrix} c_1 \\ c_2 = \dfrac{\vec{\sigma}\cdot\vec{p}_c}{2m_c}\,c_1 \end{pmatrix}$$

being developped into a large and a small component. Notice that the c quark field is a spinor of type u while the $\bar{c}$ antiquark field is of type v, so at this stage we need to express $\bar{v}$ in terms of u. Defining the charge conjugation operator by $\mathscr{C} = -i\gamma^0\gamma^2$ and using the Dirac representation for the γ matrices, we can write

$$v = \mathscr{C}(\bar{u})^T \qquad \Longrightarrow \qquad \bar{v} = (u)^T\gamma^0\mathscr{C}^\dagger\gamma^0$$

The $\bar{c}$ antiquark field is then

$$\bar{c}(\vec{p}_{\bar{c}}) \;=\; -i\left(c_1^T\,\frac{\vec{\sigma}^{\,T}\cdot\vec{p}_{\bar{c}}}{2m_c}\,\sigma_2 \;\; c_1^T\,\sigma_2\right)$$

Assuming the charmonium at rest, we have

$$\vec{p}_c = -\vec{p}_{\bar{c}} \quad \text{and} \quad (\vec{\sigma}\cdot\vec{p}_{\bar{c}})^T\sigma_2 = \sigma_2(\vec{\sigma}\cdot\vec{p}_c) \tag{2}$$

Then ordinary Pauli matrices algebra leads to

$$\begin{aligned}
\bar{c}\,\gamma^5(\vec{\gamma}\cdot\vec{\nabla})c &= \sum_{n=1}^{3} -i\left(c_1^T\,\frac{\vec{\sigma}^T\cdot\vec{p}_{\bar{c}}}{2m_c}\,\sigma_2\;\; c_1^T\,\sigma_2\right)\\
&\qquad \begin{pmatrix}-\sigma_n & 0\\ 0 & \sigma_n\end{pmatrix} D_n \begin{pmatrix} c_1 \\ \frac{\vec{\sigma}\cdot\vec{p}_c}{2m_c}\,c_1\end{pmatrix}\\
&= \sum_{n=1}^{3} c_1^T\left[-\frac{\vec{\sigma}^T\cdot\vec{p}_{\bar{c}}}{2m_c}\,\sigma_2\,\sigma_n + \sigma_2\,\sigma_n\,\frac{\vec{\sigma}\cdot\vec{p}_c}{2m_c}\right] p_{cn}\,c_1\\
&\qquad \text{assuming } D_n \sim i\;p_{cn}\\
&= \sum_{n=1}^{3} c_1^T\sigma_2\,\frac{-(\vec{\sigma}\cdot\vec{p}_c)\,\sigma_n + \sigma_n\,(\vec{\sigma}\cdot\vec{p}_c)}{2m_c}\,p_{cn}\,c_1\\
&= \sum_{n,m=1}^{3} c_1^T\sigma_2\,\frac{\sigma_n\,\sigma_m - \sigma_m\,\sigma_n}{2m_c}\,p_{cn}\,p_{cm}\,c_1\\
&= \sum_{n,m,\ell=1}^{3} i\,c_1^T\sigma_2\,\frac{\epsilon_{nm\ell}\,\sigma_\ell}{m_c}\,p_{cn}\,p_{cm}\,c_1 \;=\; 0
\end{aligned}$$

The previous approach is very naive with respect to quantum field theory, in particular the approximation $D_i c_1 \sim p_i c_1$, but as a conclusion one can see that interpolating fields $\bar{c}\,\gamma^5(\vec{\gamma}\cdot\vec{\nabla})c$ potentially give very noisy correlators. And, indeed, we have found a numerical cancellation between the "diagonal" contribution

$$A(t) = \sum_i \langle\left[\bar{c}\,\gamma^5\gamma_i\nabla_i\,c\right](t)\left[\bar{c}\,\gamma^5\gamma_i\nabla_i\,c\right](0)\,\rangle$$

and the "off-diagonal" contribution

$$B(t) = \sum_{i\neq j} \langle\left[\bar{c}\,\gamma^5\gamma_i\nabla_i\,c\right](t)\left[\bar{c}\,\gamma^5\gamma_j\nabla_j\,c\right](0)\,\rangle$$

resulting in a very noisy correlator $C(t)$ which is compatible with zero.

2.1.3 Summary

To summarise, we have considered four Gaussian smearing levels for the quark field c, including no smearing, to build 4×4 matrix of correlators without any covariant derivative nor operator of the π_2 or ρ_2 kind [24], from which we have also extracted the $\mathcal{O}(a)$ improved hadronic quantities we have examined. Solving the GEVP for the pseudoscalar-pseudoscalar and vector-vector matrices of correlators

$$\begin{aligned}
&C_{PP}(t)v_n^P(t,t_0) = \lambda_n^P(t,t_0)v_n^P(t,t_0)C_{PP}(t_0)\\
&\quad\text{and}\quad C_{VV}(t)v_n^V(t,t_0) = \lambda_n^V(t,t_0)v_n^V(t,t_0)C_{VV}(t_0)
\end{aligned} \tag{3}$$

we obtain the correlators that will have the largest overlap with the nth excited state as follows:

$$\begin{aligned}
\tilde{C}^n_{A_0P}(t) &= \sum_i C_{A_0^L P^{(i)}}(t)v_n^{P,i}(t,t_0)\\
\tilde{C}^n_{PP}(t) &= \sum_i C_{P^L P^{(i)}}(t)v_n^{P,i}(t,t_0)\\
\tilde{C}'^n_{PP}(t) &= \sum_{i,j} v_n^{P,i}(t,t_0)C_{P^{(i)}P^{(j)}}(t)v_n^{P,j}(t,t_0)\\
\tilde{C}^n_{VV}(t) &= \frac{1}{3}\sum_{i,k} C_{V_k^L V_k^{(i)}}(t)v_n^{V,i}(t,t_0)\\
\tilde{C}'^n_{VV}(t) &= \frac{1}{3}\sum_{i,j,k} v_1^{V,i}(t,t_0)C_{V_k^{(i)}V_k^{(j)}}(t)v_n^{V,j}(t,t_0)\\
\tilde{C}^n_{TV}(t) &= \frac{1}{3}\sum_{i,k} C_{T_{k0}^L V_k^{(i)}}(t)v_n^{V,i}(t,t_0)\\
\tilde{C}^n_{\delta PP}(t) &= \frac{\tilde{C}^n_{PP}(t+1) - \tilde{C}^n_{PP}(t-1)}{2a}\\
\tilde{C}^n_{\delta TV}(t) &= \frac{\tilde{C}^n_{TV}(t+1) - \tilde{C}^n_{TV}(t-1)}{2a}
\end{aligned}$$

and their symmetric counterpart with the exchange of operators at the source and at the sink. The quark bilinears are $P = \bar{c}\gamma_5 c$, $A_0 = \bar{c}\gamma_0\gamma_5 c$, $V_k = \bar{c}\gamma_k c$ and $T_{k0} = \bar{c}\gamma_k\gamma_0 c$. Moreover, in those expressions, the label L refers to a local interpolating field while sums over i and j run over the four Gaussian smearing levels.

The projected correlators have the following asymptotic behaviour

$$\begin{aligned}
\tilde{C}'^n_{PP}(t) &\xrightarrow[t/a\gg 1]{} \frac{\mathcal{Z}'_{PP_n}}{am_{P_n}}e^{-m_{P_n}T/2}\cosh[m_{P_n}(T/2-t)]\\
\tilde{C}^n_{A_0P}(t) &\xrightarrow[t/a\gg 1]{} -\frac{\mathcal{Z}_{AP_n}}{am_{P_n}}e^{-m_{P_n}T/2}\sinh[m_{P_n}(T/2-t)]\\
\tilde{C}^n_{PP}(t) &\xrightarrow[t/a\gg 1]{} \frac{\mathcal{Z}_{PP_n}}{am_{P_n}}e^{-m_{P_n}T/2}\cosh[m_{P_n}(T/2-t)]\\
\tilde{C}'^n_{VV}(t) &\xrightarrow[t/a\gg 1]{} \frac{\mathcal{Z}'_{VV_n}}{am_{V_n}}e^{-m_{V_n}T/2}\cosh[m_{V_n}(T/2-t)]\\
\tilde{C}^n_{VV}(t) &\xrightarrow[t/a\gg 1]{} \frac{\mathcal{Z}_{VV_n}}{am_{V_n}}e^{-m_{V_n}T/2}\cosh[m_{V_n}(T/2-t)]\\
\tilde{C}^n_{TV}(t) &\xrightarrow[t/a\gg 1]{} \frac{\mathcal{Z}_{TV_n}}{am_{V_n}}e^{-m_{V_n}T/2}\sinh[m_{V_n}(T/2-t)]\\
\tilde{C}^n_{\delta PP}(t) &\xrightarrow[t/a\gg 1]{} -1/a\;\sinh(am_{P_n})\frac{\mathcal{Z}_{PP_n}}{am_{P_n}}e^{-m_{P_n}T/2}\\
&\quad \sinh[m_{P_n}(T/2-t)]\\
\tilde{C}^n_{\delta TV}(t) &\xrightarrow[t/a\gg 1]{} -1/a\;\sinh(am_{V_n})\frac{\mathcal{Z}_{TV_n}}{am_{V_n}}e^{-m_{V_n}T/2}\\
&\quad \cosh[m_{V_n}(T/2-t)]
\end{aligned}$$

2.1.4 Decay constant extraction

Considering the $\mathcal{O}(a)$ improved operators

$$A_0^I = (1 + b_A Z a m_c^{AWI}) \left(A_0 + a c_A \frac{\partial_0 + \partial_0^*}{2} P \right) \quad \text{and}$$
$$V_k^I = (1 + b_V Z a m_c^{AWI}) \left(V_k + a c_V \frac{\partial_\nu + \partial_\nu^*}{2} T_{k\nu} \right) \tag{4}$$

where the lattice derivatives are defined by

$$\partial_\nu F(x) = \frac{F(x + a\hat{\nu}) - F(x)}{a} \quad \text{as well as}$$
$$\partial_\nu^* F(x) = \frac{F(x) - F(x - a\hat{\nu})}{a}, \tag{5}$$

the f_{η_c} decay constants is extracted in the following way:

$$\begin{cases} \langle 0 \mid A_0^R \mid \eta_c(\vec{p} = 0) \rangle = -f_{\eta_c} m_{\eta_c} \\ \quad = -Z_A (1 + b_A Z a m_c^{AWI}) m_{\eta_c} f_{P_c}^0 (1 + f_{P_c}^1 / f_{P_c}^0) \\ a f_{P_c}^0 = \frac{1}{a m_{\eta_c}} \frac{\mathcal{Z}_{AP_1}}{\sqrt{\mathcal{Z}'_{PP_1}}}; \quad a f_{P_c}^1 = \frac{1}{a m_{\eta_c}} c_A \sinh(a m_{\eta_c}) \frac{\mathcal{Z}_{PP_1}}{\sqrt{\mathcal{Z}'_{PP_1}}} \end{cases} \tag{6}$$

while the $f_{J/\psi}$ decay constant is obtained with:

$$\begin{cases} \langle 0 \mid V_i^R \mid J/\psi(\epsilon, \vec{p} = 0) \rangle = \epsilon_i f_{J/\psi} m_{J/\psi} \\ \quad = \epsilon_i Z_V (1 + b_V Z a m_c^{AWI}) m_{J/\psi} f_{V_c}^0 (1 + f_{V_c}^1 / f_{V_c}^0) \\ a f_{V_c}^0 = \frac{1}{a m_{J/\psi}} \frac{\mathcal{Z}_{VV_1}}{\sqrt{\mathcal{Z}'_{VV_1}}}; \qquad a f_{V_c}^1 \\ \quad = -\frac{1}{a m_{J/\psi}} c_V \sinh(a m_{J/\psi}) \frac{\mathcal{Z}_{TV_1}}{\sqrt{\mathcal{Z}'_{VV_1}}} \end{cases} \tag{7}$$

The R superscript denotes the renormalized improved operators. The renormalization constants Z_A and Z_V have been non perturbatively measured in [26,27].[1] We have also used non-perturbative results and perturbative formulae from [28–30] for the improvement coefficients c_A, c_V, b_A and b_V, and the matching coefficient Z between the quark mass m_c defined through the axial Ward Identity

$$m_c^{AWI} = \frac{\frac{\partial_0 + \partial_0^*}{2} C_{A_0^L P^L}(t) + a c_A \partial_0 \partial_0^* C_{P^L P^L}(t)}{2 C_{P^L P^L}(t)}$$

and its counterpart defined through the vector Ward Identity

$$a m_c^{VWI} = \frac{1}{2} \left(\frac{1}{\kappa_c} - \frac{1}{\kappa_{cr}} \right)$$

The decay constants of the considered radial excited states are given by

$$\begin{cases} \langle 0 \mid A_0^R \mid \eta_c(2S)(\vec{p} = 0) \rangle = -f_{\eta_c(2S)} m_{\eta_c(2S)} \\ \quad = -Z_A (1 + b_A Z a m_c^{AWI}) m_{\eta_c(2S)} f_{P_c'}^0 (1 + f_{P_c'}^1 / f_{P_c'}^0) \\ a f_{P_c'}^0 = \frac{1}{a m_{\eta_c(2S)}} \frac{\mathcal{Z}_{AP_2}}{\sqrt{\mathcal{Z}'_{PP_2}}}; \\ \quad a f_{P_c'}^1 = \frac{1}{a m_{\eta_c(2S)}} c_A \sinh(a m_{\eta_c(2S)}) \frac{\mathcal{Z}_{PP_2}}{\sqrt{\mathcal{Z}'_{PP_2}}} \end{cases} \tag{8}$$

and

$$\begin{cases} \langle 0 \mid V_i^R \mid \psi(2S)(\epsilon, \vec{p} = 0) \rangle = \epsilon_i f_{\psi(2S)} m_{\psi(2S)} \\ \quad = \epsilon_i Z_V (1 + b_V Z a m_c^{AWI}) m_{\psi(2S)} f_{V_c'}^0 (1 + f_{V_c'}^1 / f_{V_c'}^0) \\ a f_{V_c'}^0 = \frac{1}{a m_{\psi(2S)}} \frac{\mathcal{Z}_{VV_2}}{\sqrt{\mathcal{Z}'_{VV_2}}}; \\ \quad a f_{V_c'}^1 = -\frac{1}{a m_{\psi(2S)}} c_V \sinh(a m_{\psi(2S)}) \frac{\mathcal{Z}_{TV_2}}{\sqrt{\mathcal{Z}'_{VV_2}}} \end{cases} \tag{9}$$

2.2 Analysis

Let us first consider the mass and the decay constant of the ground states. Since the fluctuations on effective masses obtained from $\tilde{C}^1_{A_0 P}$ and C^1_{VV} are large with time, we have decided to use generalized eigenvectors *at fixed time* $t_{\rm fix}$, $v_1^{P(V)}(t_{\rm fix}, t_0)$, in order to perform the corresponding projections. In practice we have chosen $t_{\rm fix}/a = t_0/a + 1$ but we have checked that the results do not depend on $t_{\rm fix}$.

For the excited states, the formulae written in Sect. 2.1.3 do apply. Although the fluctuations on effective masses obtained from $\tilde{C}^2_{A_0 P}$ and $\tilde{C}^2_{VV}$ are larger than for their ground states counterparts, the correlators $\tilde{C}^2_{A_0 P}$ and $\tilde{C}^2_{VV}$ computed with a projection on $v_2^{P(V)}(t_{\rm fix}, t_0)$ show a bigger slope than the same correlators computed with a projection on $v_2^{P(V)}(t, t_0)$. We interpret that observation as a stronger contamination of higher excited states for the $t_{\rm fix}$ projection which can spoil the determination of the $\eta_c(2S)$ and $\psi(2S)$ masses. Since the masses take part in the computation of the decay constants, such a contamination can propagate into the extraction of $f_{\eta_c(2S)}$ and $f_{\psi(2S)}$. Figures 2 and 3 illustrate that point with the correlators $\tilde{C}^2_{A_0 P}$ and $\tilde{C}^2_{VV}$ on the ensemble F7.

For the ground states, the time range $[t_{\rm min}, t_{\rm max}]$ used to fit the projected correlators is set so that the statistical error on the effective mass $\delta m^{\rm stat}(t_{\rm min})$ is larger enough than the systematic error $\Delta m^{\rm sys}(t_{\rm min}) \equiv \exp[-\Delta t_{\rm min}]$ with $\Delta = E_4 - E_1 \sim 2$ GeV. That guesstimate is based on our 4×4 GEVP analysis, though we do not want to claim here that we really control the

[1] Z_A is the finite renormalisation constant of a flavour non-singlet axial bilinear of quarks: it is different from 1 because Wilson-Clover fermions break the chiral symmetry. In that work we consider flavour singlet operators: due to the chiral anomaly the renormalisation pattern is different. However the feature of flavour symmetry (singlet vs. non-singlet) is intimately related to the chiral symmetry. As the charm quark is not chiral at all, its sensitivity to the chiral anomaly is negligible. Hence it is acceptable to renormalise the operator $\bar{c}\gamma_0\gamma_5 c$ with the "flavour non-singlet" renormalisation constant Z_A.

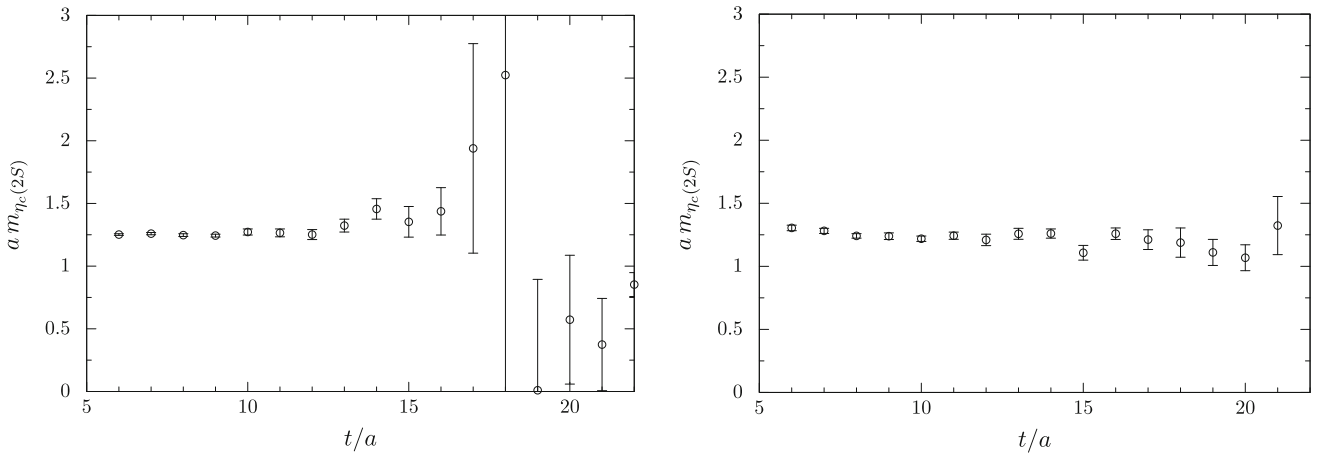

Fig. 2 Effective mass of the $\eta_c(2S)$ state extracted from the correlator $\tilde{C}^2_{A_0P}$ computed using either a fixed time $t_{\rm fix}$ (left plot) or a running time t (right plot) to project $C_{A_0^L P}$ along the ground state generalized eigenvector v_2^P

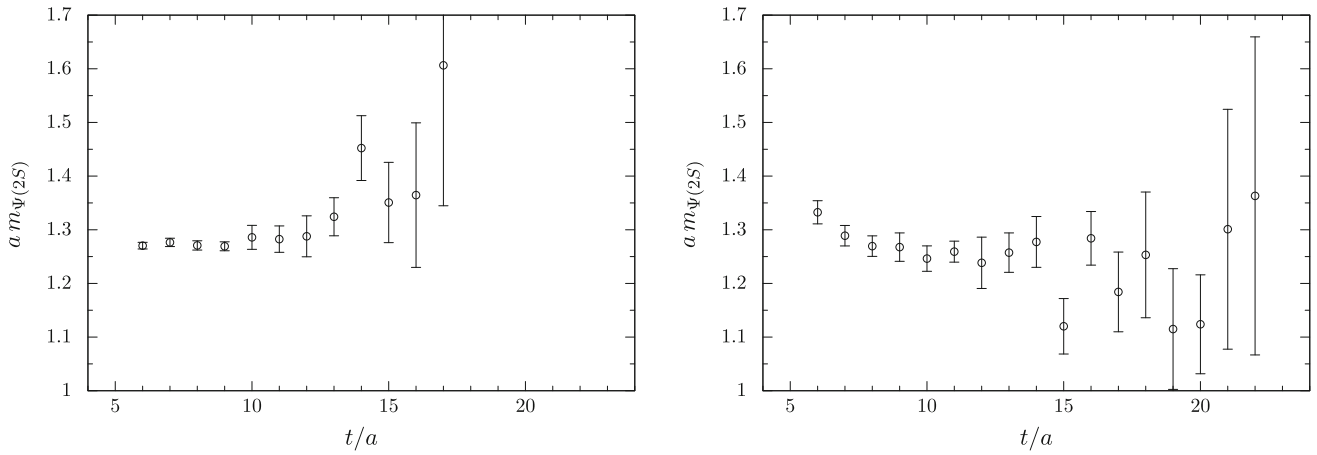

Fig. 3 Effective mass of the $\psi(2S)$ state extracted from the correlator $\tilde{C}^2_{VV}$ computed using either a fixed time $t_{\rm fix}$ (left plot) or a running time t (right plot) to project $C_{V^L V}$ along the first excited state generalized eigenvector v_2^V

energy-level of the third excited state. Actually our criterion is rather $\delta m^{\rm stat}(t_{\rm min}) > 4\Delta m^{\rm sys}(t_{\rm min})$ to be more conservative. On the other side, $t_{\rm max}$ is set after a qualitative inspection of the data which count for the plateau determination. Since $\Delta^{(P)} \sim \Delta^{(V)}$, fit intervals are identical for pseudoscalar and vector charmonia.

For the first excited states, the time range has been set by looking at effective masses and where the plateaus start and end, including statistical uncertainty. There, we have estimated the systematic error by shifting the fit range to larger times $[t_{\rm min}, t_{\rm max}] \to [t_{\rm min} + 2a, t_{\rm max} + 3a]$.

Finally, we have taken $t_0 = 3a$ at $\beta = 5.3$ and $t_0 = 5a$ at $\beta = 5.5$: the landscape is unchanged by increasing t_0. The raw data we have obtained in our analysis is collected in Table 3 of the Appendix. The extrapolation to the physical point of the quantities we have measured uses a linear expression in m_π^2 with inserted cut-off effects in a^2:

$$X(a, m_\pi) = X_0 + X_1 m_\pi^2 + X_2 (a/a_{\beta=5.3})^2 \tag{10}$$

We remind that κ_c have been tuned at every $\kappa_{\rm sea}$ so that $m_{D_s}(\kappa_s, \kappa_c, \kappa_{\rm sea}) = m_{D_s}^{\rm phys}$ (it was necessary to tune the strange quark mass κ_s, though it is not a relevant quantity for the study discussed here).

Figure 4 shows the effective masses of the η_c, $\eta_c(2S)$, J/ψ and $\psi(2S)$ mesons for the set F7 which are obtained by the following expressions

$$\begin{cases} am^{\rm eff}_{\eta_c}(t) &= \text{argcosh}\left(\frac{\lambda_1^P(t+a,t_0)+\lambda_1^P(t-a,t_0)}{2\lambda_1^P(t,t_0)}\right) \\ am^{\rm eff}_{J/\psi}(t) &= \text{argcosh}\left(\frac{\lambda_1^V(t+a,t_0)+\lambda_1^V(t-a,t_0)}{2\lambda_1^V(t,t_0)}\right) \end{cases}$$

and

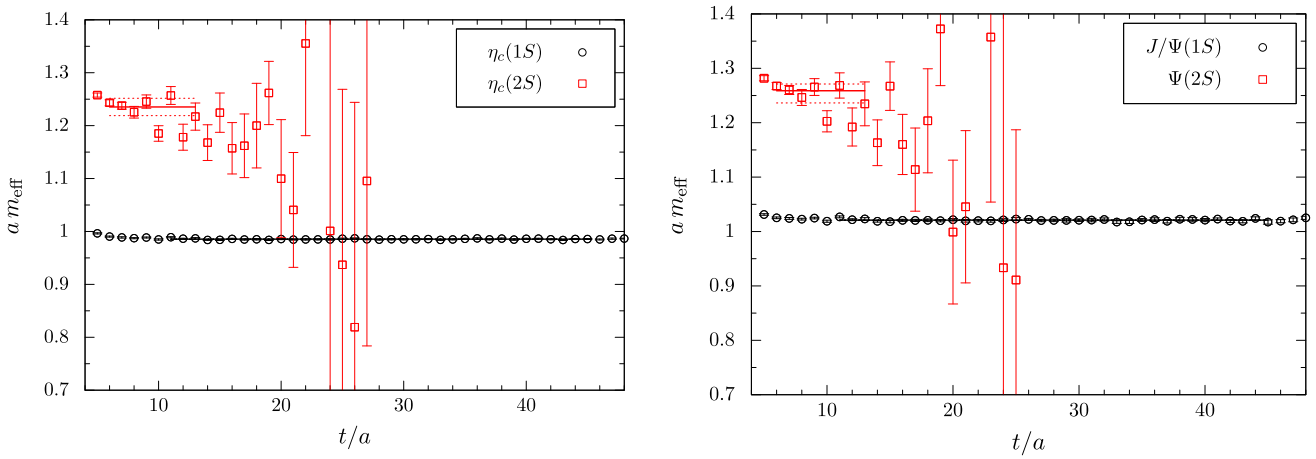

Fig. 4 Effective masses am_{η_c} and $am_{\eta_c(2S)}$ (left panel), $am_{J/\psi}$ and $am_{\psi(2S)}$ (right panel) extracted from a 4×4 GEVP for the lattice ensemble F7; we also plot the plateaus obtained in the chosen fit interval

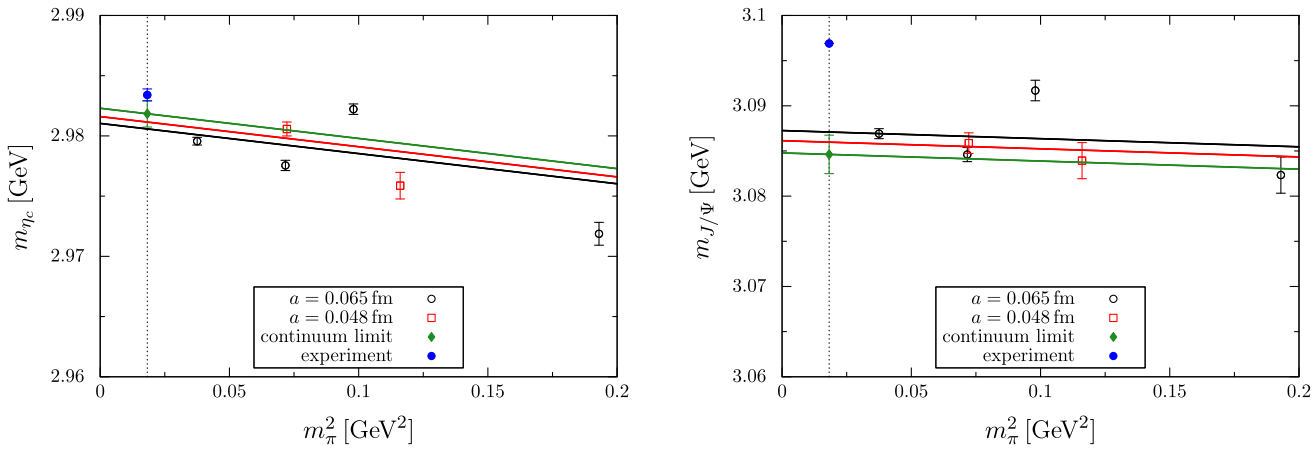

Fig. 5 Extrapolation at the physical point of m_{η_c} (left panel) and $m_{J/\psi}$ (right panel) by linear expressions in m_π^2 and a^2

$$\begin{cases} am^{\rm eff}_{\eta_c(2S)}(t) &= \text{argcosh}\left(\frac{\lambda_2^P(t+a,t_0)+\lambda_2^P(t-a,t_0)}{2\lambda_1^P(t,t_0)}\right) \\ am^{\rm eff}_{\psi(2S)}(t) &= \text{argcosh}\left(\frac{\lambda_2^V(t+a,t_0)+\lambda_2^V(t-a,t_0)}{2\lambda_1^V(t,t_0)}\right) \end{cases}$$

The drawn lines correspond to our plateaus for the fitted masses. One can observe that our plateaus are large for the ground states but they are unfortunately of a much worse quality for the radial excitations. The latter data also show large fluctuations with time, for which we did not find any satisfying explanation yet. If $t_{\rm fix}$ were used in the correlators projection procedure, the price to pay would be a strong contamination by other states in $\tilde{C}^2_{A_0P}$ and $\tilde{C}^2_{VV}$ other than the ones of interest.

2.2.1 Ground state results

We show in Fig. 5 the extrapolation to the physical point of m_{η_c} and $m_{J/\psi}$. The dependence on m_π^2 and a^2 is mild, with cut-off effects almost negligible. However the contribution to the meson masses besides the mass term $2m_c$ is difficult to catch. All in all, there is a variation of m_{η_c} and $m_{J/\psi}$ smaller than 100 MeV, i.e. smaller than 3% of the mass, for the different lattice ensembles. This creates a sort of zoom effect on the fluctuations (they are at least 2 orders of magnitude larger than the statistical error) which explains why the quality of the fit seems poor. At the physical point, m_{η_c} and $m_{J/\psi}$ are compatible with the experimental values 2.983 GeV and 3.097 GeV:

$$m_{\eta_c} = 2.982(1)(19)\,\text{GeV} \quad \text{and} \quad m_{J/\psi} = 3.085(2)(20)\,\text{GeV} \tag{11}$$

where the first error is statistical and the second error accounts for the uncertainty on the lattice spacing. The latter clearly dominates and hides a possible mismatch between our extrapolated results at the physical point and experiment, in particular coming from the mistuning of κ_c due to the mistuning of κ_s.

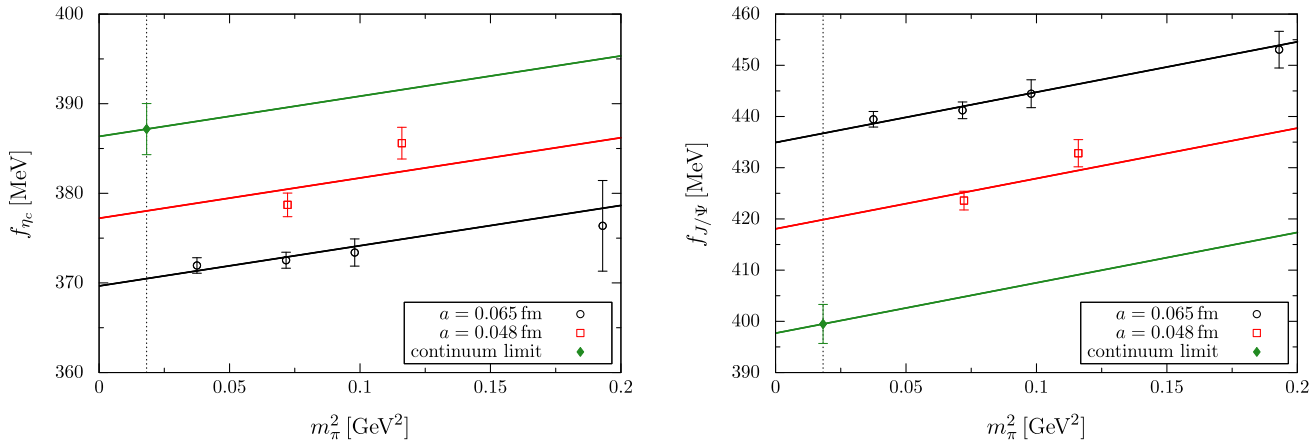

Fig. 6 Extrapolation at the physical point of f_{η_c} (left panel) and $f_{J/\psi}$ (right panel) by linear expressions in m_π^2 and a^2

Table 2 LO and NLO fit parameters and results for f_{η_c} and $f_{J/\psi}$, with their respective χ^2 per degrees of freedom

Fit	X_0[MeV]	X_1 [MeV^{-1}]	X_2 [MeV]	X_3 [MeV^{-1}]	χ^2/dof	f_{η_c}
LO	386(3)	0.00005(1)	−16.7(2.7)	–	1.99	387(3)
NLO	391(6)	0.0006(7)	−17.1(2.7)	0.00006(6)	2.62	389(4)
Fit	X_0 [MeV]	X_1 [MeV^{-1}]	X_2 [MeV]	X_3 [MeV^{-1}]	χ^2/dof	$f_{J/\psi}$
LO	397(4)	0.00010(2)	37.2(3.8)	–	0.98	399(4)
NLL	401(7)	−0.0003(9)	36.4(4.2)	0.00003(7)	1.41	401(8)

We display in Fig. 6 the extrapolations at the physical point of f_{η_c} and $f_{J/\psi}$. They are mild and cut-off effects on f_{η_c} are of the order of 4% at $\beta = 5.3$ while they are stronger for $f_{J/\psi}$, about 10%. In addition to the fit formula Eq. (10) we have tried to fit our data with an "NLO" ansatz,

$$\begin{aligned} f_{\eta_c} &= X'_{\eta_c 0} + X'_{\eta_c 1} m_\pi^2 + X'_{\eta_c 2}(a/a_{\beta=5.3})^2 \\ &\quad + X'_{\eta_c 3} m_\pi^2 \ln m_\pi^2, \\ f_{J/\psi} &= X'_{J/\psi 0} + X'_{J/\psi 1} m_\pi^2 + X'_{J/\psi 2}(a/a_{\beta=5.3})^2 \\ &\quad + X'_{J/\psi 3} m_\pi^2 \ln m_\pi^2. \end{aligned} \tag{12}$$

We have collected in Table 2 results of the LO and NLO fits, together with fit parameters and χ^2 per degree of freedom. As χ^2(NLO) is worse than χ^2(LO) and the fit parameters X'_1 and X'_3 are compatible with zero, while X_1 is different from zero, we have decided to consider the LO result as our prefered one and not include the discrepancy between (LO) and (NLO) in the systematic error on f_{η_c} and $f_{J/\psi}$. We do not have enough data points to be really confident in (NLO) fits on quantities whose chiral dependence is small anyway.

We get at the physical point

$$f_{\eta_c} = 387(3)(3)\,\text{MeV} \quad \text{and} \quad f_{J/\psi} = 399(4)(2)\,\text{MeV}, \tag{13}$$

where the systematic error comes from the uncertainty on lattice spacings.

Moreover, one can derive a phenomenological estimate of $f_{J/\psi}$. Indeed, using the expression of the electronic decay width

$$\Gamma(J/\psi \to e^+e^-) = \frac{4\pi}{3}\frac{4}{9}\alpha^2(m_c^2)\frac{f_{J/\psi}^2}{m_{J/\psi}}$$

together with the experimental determination of the J/ψ mass and width, and setting $\alpha_{\text{em}}(m_c^2) = 1/134$ [31,32], one gets

$$f_{J/\psi}^{\text{"exp"}} = 407(6)\,\text{MeV}$$

We collect the various lattice QCD results and the phenomenological estimate of $f_{J/\psi}$ in Fig. 7.

2.2.2 *First radial excitation results*

The situation is, unfortunately, less favorable with the excited states. Figure 8 shows the extrapolation to the continuum limit of the ratios $m_{\eta_c(2S)}/m_{\eta_c}$ and $m_{\psi(2S)}/m_{J/\psi}$, compared to the experimental values. Since the cut-off effects are small, of the order of 5%, there is no hope to have points in the continuum limit significantly lower than our lattice data. We get

$$m_{\eta_c(2S)}/m_{\eta_c} = 1.279(6) \gg (m_{\eta_c(2S)}/m_{\eta_c})^{\text{exp}} = 1.220$$

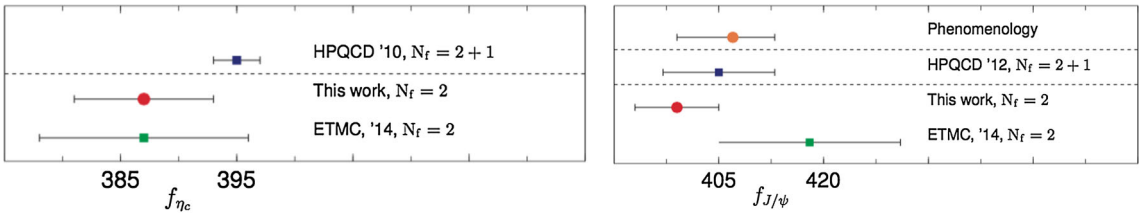

Fig. 7 Collection of lattice results of f_{η_c} (left panel) and $f_{J/\psi}$ (right panel)

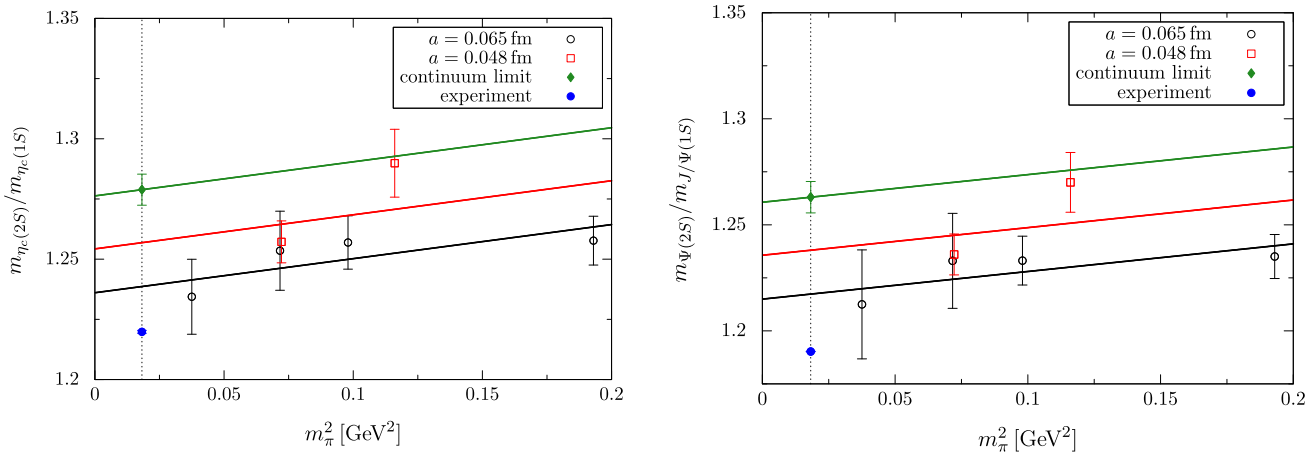

Fig. 8 Extrapolation at the physical point of $m_{\eta_c(2S)}/m_{\eta_c}$ (left panel) and $m_{\psi(2S)}/m_{J/\psi}$ (right panel) by linear expressions in m_π^2 and a^2. Errors include the systematic error obtained by changing the time range to fit $m_{\eta_c(2S)}$ and $m_{\psi(2S)}$ as described in Sect. 2.2

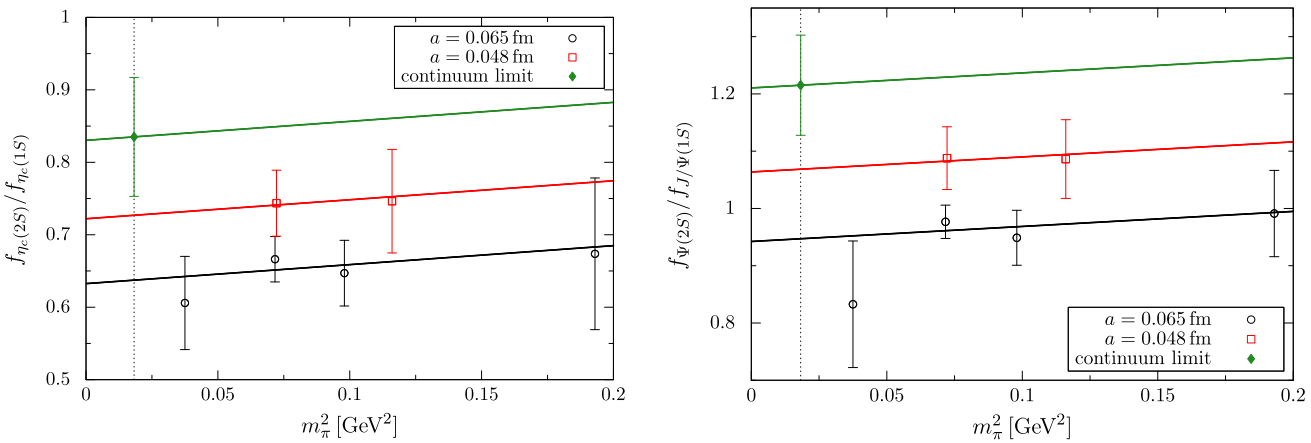

Fig. 9 Extrapolation at the physical point of $f_{\eta_c(2S)}/f_{\eta_c}$ (left panel) and $f_{\psi(2S)}/f_{J/\psi}$ (right panel) by linear expressions in m_π^2 and a^2. Errors include the systematic error obtained by changing the time range to fit $f_{\eta_c(2S)}$ and $f_{\psi(2S)}$ as described in Sect. 2.2

and

$$m_{\psi(2S)}/m_{J/\psi} = 1.263(7) \gg (m_{\psi(2S)}/m_{J/\psi})^{\text{exp}} = 1.190$$

In [33], lattice results were much closer to the experiment but the slope in a^2 was probably overrestimated from the coarsest lattice point: points at lattice spacings similar to those used in our work are compatible with our data.

The situation is even more confusing for the ratios of decay constants, as shown in Fig. 9

$$f_{\eta_c(2S)}/f_{\eta_c} = 0.84(8) < 1 \quad \text{while}$$
$$f_{\psi(2S)}/f_{J/\psi} = 1,22(9) > 1$$

We have not found any explanation for such a large spin breaking effect. Projected correlators $\tilde{C}^2$ in the pseudoscalar and the vector sector show the same quality fit with similar fluctuations. We also have performed a global fit of individual correlators $C_{V^{(i)}V^{(j)}}(t)$ by a series of 3 exponential contributions

$$\begin{aligned} C_{V^{(i)}V^{(j)}}(t) = & Z_1^i Z_1^{*j} e^{-m_{V_1} T/2} \cosh[m_{V_1}(T/2-t)] \\ & + Z_2^i Z_2^{*j} e^{-m_{V_2} T/2} \cosh[m_{V_2}(T/2-t)] \\ & + Z_3^{ij} e^{-m_3^{ij} T/2} \cosh[m_3^{ij}(T/2-t)] \end{aligned}$$

where the "effective" remaining mass m_3, resumming any contributions but the ground state and the first excited state, can be different for every correlator. Decay constants of J/ψ and $\psi(2S)$ are proportional to $Z_1^0/\sqrt{m_{V_1}}$ and $Z_2^0/\sqrt{m_{V_2}}$ (the local-local vector 2-pt correlator corresponds to $i = j = 0$) and we find the hierarchy $Z_2^0/\sqrt{m_{V_2}} \gtrsim Z_1^0/\sqrt{m_{V_1}}$ in our sets of data. There is no hope to get in the continuum limit $f_{\psi(2S)}/f_{J/\psi} < 1$ using this procedure either. Neglecting disconnected diagrams could be a source of the problem and including more flavours in the sea might help reduce the spin breaking effects, as it was observed on quantities like $f_{D_s^*}/f_{D_s}$ [35–38]. Moreover, the width $\Gamma(\psi(2S) \to e^+e^-)$ is smaller than its ground state counterpart $\Gamma(J/\psi \to e^+e^-)$, that is 2.34 keV versus 5.56 keV [34]; written in terms of the decay constant $f_{\psi(2S)}$ and the mass $m_{\psi(2S)}$, this is a serious clue that $f_{\psi(2S)}/f_{J/\psi} < 1$.[2] In addition, a lattice study, performed in the framework of NRQCD, gives $f_{\Upsilon'}/f_{\Upsilon} < 1$ in the bottomium sector [39].

3 Conclusion

In that paper we have reported a $N_f = 2$ lattice QCD study about the physics of quarkonia. The decay constants f_{η_c} and $f_{J/\psi}$ are in the same ballpark as the two previous lattice estimations available so far in the literature, with the good news that cut-off effects seem to be limited to 10%. The issues with radial excitations are difficult to circumvent. As a first solution, the basis of operators in the GEVP analysis could be enlarged by including interpolating fields with covariant derivatives or operators of the π_2 and ρ_2 kind. But both of them suffer either from big statistical fluctuations, because of numerical cancellation among various contributions, or from the more serious conceptual problem that, in GEVP, mixing T-even and T-odd operators has no real sense. Second, $m_{\eta_c(2S)}/m_{\eta_c}$ and $m_{\psi(2S)}/m_{J/\psi}$ are not significantly affected by cut-off effects, so that they are 5% larger than the experimental ratios. The information that $f_{\eta_c(2S)}/f_{\eta_c} \sim 0.8$ is interesting, as the decay constants f_{η_c} and $f_{\eta_c(2S)}$ are hadronic inputs that govern the transitions $\eta_c \to l^+l^-$, $h \to \eta_c l^+l^-$, $\eta_c(2S) \to l^+l^-$ and $h \to \eta_c(2S)l^+l^-$ with a light CP-odd Higgs boson as an intermediate state.[3] Unfortunately, our result for $f_{\psi(2S)}/f_{J/\psi} > 1$ makes the picture less bright, unless one admits that there are very large spin breaking effects. Further investigation to address this issue is undoubtedly required.

Meanwhile, the next step into the measurement of f_{η_b}, particularly relevant in models with a light CP-odd Higgs, is underway using step scaling in masses in order to extrapolate the results to the bottom region.

Acknowledgements This work was granted access to the HPC resources of CINES and IDRIS under the allocations 2016-x2016056808 and 2017-A0010506808 made by GENCI. It is supported by Agence Nationale de la Recherche under the contract ANR-17-CE31-0019. Authors are grateful to Damir Becirevic and Olivier Pène for useful discussions and the colleagues of the CLS effort for having provided the gauge ensembles used in that work.

Funded by SCOAP[3].

Appendix

We collect in Table 3 the values of η_c and J/ψ masses and decay constants extracted at each ensemble of our analysis, as well as the ratios of masses and decay constants $m_{\eta_c(2S)}/m_{\eta_c}$, $m_{\psi(2S)}/m_{J/\psi}$, $f_{\eta_c(2S)}/f_{\eta_c}$ and $f_{\psi(2S)}/f_{J/\psi}$.

[2] A possible caveat with this approach is that QED effects might be quite large, making, as is done in our work, the encoding in $f_{\psi(2S)}$ as purely QCD contributions not so straightforward.

[3] In the cases $h \to \eta_c l^+l^-$ and $h \to \eta_c(2S)l^+l^-$, the other hadronic quantities which enter the process are the distribution amplitudes of the charmonia.

Table 3 Masses and decays constants of η_c, $\eta_c(2S)$, J/ψ and $\psi(2S)$, in lattice units, extracted on each CLS ensemble used in our analysis

id	$[t_{\min}, t_{\max}](P)$	am_{η_c}	af_{η_c}	$[t_{\min}, t_{\max}](V)$	$am_{J/\psi}$	$af_{J/\psi}$
E5	[11–29]	0.9836(3)	0.1246(16)	[11-29]	1.0202(7)	0.1499(11)
F6	[11–46]	0.9870(1)	0.1236(5)	[11-46]	1.0233(4)	0.1471(9)
F7	[11–45]	0.9855(1)	0.1233(3)	[11-45]	1.0209(3)	0.1460(5)
G8	[12–55]	0.9861(1)	0.1231(3)	[12-55]	1.0217(2)	0.1454(5)
N6	[13–46]	0.7284(3)	0.0944(6)	[13-46]	0.7547(6)	0.1059(8)
O7	[16–55]	0.7297(1)	0.0927(3)	[16-55]	0.7555(3)	0.1037(4)
id	$[t_{\min}, t_{\max}](P')$	$m_{\eta_c(2S)/m_{\eta_c}}$	$f_{\eta_c(2S)}/f_{\eta_c}$	$[t_{\min}, t_{\max}](V')$	$m_{\psi(2S)}/m_{J/\psi}$	$f_{\psi(2S)}/f_{J/\psi}$
E5	[6–13]	1.258(5)(5)	0.67(10)(6)	[6Th-13]	1.235(5)(5)	0.99(6)(7)
F6	[6–13]	1.257(3)(8)	0.65(4)(5)	[6-13]	1.233(4)(8)	0.95(4)(3)
F7	[6–13]	1.254(2)(14	0.67(2)(14)	[6-13]	1.233(3)(19)	0.98(2)(5)
G8	[8–15]	1.234(12)(4)	0.61(6)(2)	[8-15]	1.212(18)(7)	0.83(10)(8)
N6	[8–15]	1.290(4)(10)	0.75(6)(9)	[8-15]	1.270(4)(10)	1.09(7)(2)
O7	[8–15]	1.257(4)(5)	0.74(4)(5)	[8-15]	1.236(5)(5)	1.09(5)(3)

References

1. G. Aad et al., [ATLAS and CMS Collaborations], Phys. Rev. Lett. **114**, 191803 (2015). arXiv:1503.07589 [hep-ex]
2. E. Fullana, M.A. Sanchis-Lozano, Phys. Lett. B **653**, 67 (2007). arXiv:hep-ph/0702190
3. D. Becirevic, B. Melic, M. Patra, O. Sumensari. arXiv:1705.01112 [hep-ph]
4. L. Liu et al., [Hadron Spectrum Collaboration], JHEP **1207**, 126 (2012). arXiv:1204.5425 [hep-ph]
5. C.B. Lang, L. Leskovec, D. Mohler, S. Prelovsek, JHEP **1509**, 089 (2015). arXiv:1503.05363 [hep-lat]
6. D. Becirevic, G. Duplancic, B. Klajn, B. Melic, F. Sanfilippo, Nucl. Phys. B **883**, 306 (2014). arXiv:1312.2858 [hep-ph]
7. C.T.H. Davies, C. McNeile, E. Follana, G.P. Lepage, H. Na, J. Shigemitsu, Phys. Rev. D **82**, 114504 (2010). arXiv:1008.4018 [hep-lat]
8. G.C. Donald, C.T.H. Davies, R.J. Dowdall, E. Follana, K. Hornbostel, J. Koponen, G.P. Lepage, C. McNeile, Phys. Rev. D **86**, 094501 (2012). arXiv:1208.2855 [hep-lat]
9. B. Sheikholeslami, R. Wohlert, Nucl. Phys. B **259**, 572 (1985)
10. M. Lüscher, S. Sint, R. Sommer, P. Weisz, U. Wolff, Nucl. Phys. B **491**, 323 (1997). arXiv:hep-lat/9609035
11. K.G. Wilson, Phys. Rev. D **10**, 2445 (1974)
12. M. Lüscher, Comput. Phys. Commun. **156**, 209 (2004). arXiv:hep-lat/0310048
13. M. Lüscher, Comput. Phys. Commun. **165**, 199 (2005). arXiv:hep-lat/0409106
14. M. Lüscher, JHEP **0712**, 011 (2007). arXiv:0710.5417 [hep-lat]
15. M. Lüscher, DD-HMC algorithm for two-flavour lattice QCD. http://luscher.web.cern.ch/luscher/DD-HMC/index.html
16. M. Marinkovic, S. Schaefer, PoS LATTICE **2010**, 031 (2010). arXiv:1011.0911 [hep-lat]
17. S. Lottini [ALPHA Collaboration], PoS LATTICE **2013**, 315 (2014). arXiv:1311.3081 [hep-lat]
18. J. Heitger, G.M. von Hippel, S. Schaefer, F. Virotta, PoS LATTICE **2013**, 475 (2014). arXiv:1312.7693 [hep-lat]; J. Heitger, private communication
19. P. Fritzsch, F. Knechtli, B. Leder, M. Marinkovic, S. Schaefer, R. Sommer, F. Virotta, Nucl. Phys. B **865**, 397 (2012). arXiv:1205.5380 [hep-lat]
20. M. Foster, UKQCD Collaboration. Phys. Rev. D **59**, 094509 (1999). arXiv:hep-lat/9811010
21. C. McNeile, UKQCD Collaboration. Phys. Rev. D **73**, 074506 (2006). arXiv:hep-lat/0603007
22. C. Michael, Nucl. Phys. B **259**, 58 (1985)
23. M. Lüscher, U. Wolff, Nucl. Phys. B **339**, 222 (1990)
24. J.J. Dudek, R.G. Edwards, M.J. Peardon, D.G. Richards, C.E. Thomas, Phys. Rev. D **82**, 034508 (2010). arXiv:1004.4930 [hep-ph]
25. D. Mohler, S. Prelovsek, R. M. Woloshyn, Phys. Rev. D **87**(3), 034501 (2013). arXiv:1208.4059 [hep-lat]
26. M. Della Morte, R. Sommer, S. Takeda, Phys. Lett. B **672**, 407 (2009). arXiv:0807.1120 [hep-lat]
27. M. Della Morte, R. Hoffmann, F. Knechtli, R. Sommer, U. Wolff, JHEP **0507**, 007 (2005). arXiv:hep-lat/0505026
28. M. Della Morte, R. Hoffmann, R. Sommer, JHEP **0503**, 029 (2005). arXiv:hep-lat/0503003
29. S. Sint, P. Weisz, Nucl. Phys. B **502**, 251 (1997). arXiv:hep-lat/9704001
30. M. Guagnelli et al., [ALPHA Collaboration], Nucl. Phys. B **595**, 44 (2001). arXiv:hep-lat/0009021
31. A.A. Pivovarov, Phys. Atom. Nucl. **65**, 1319 (2002)
32. A.A. Pivovarov, Yad. Fiz. **65**, 1352 (2002). arXiv:hep-ph/0011135
33. D. Becirevic, M. Kruse, F. Sanfilippo, JHEP **1505**, 014 (2015). arXiv:1411.6426 [hep-lat]
34. C. Patrignani et al. [Particle Data Group], Chin. Phys. C **40**(10), 100001 (2016)
35. D. Becirevic, V. Lubicz, F. Sanfilippo, S. Simula, C. Tarantino, JHEP **1202**, 042 (2012). arXiv:1201.4039 [hep-lat]
36. B. Blossier, J. Heitger, M. Post. arXiv:1803.03065 [hep-lat]
37. G.C. Donald, C.T.H. Davies, J. Koponen, G.P. Lepage, Phys. Rev. Lett. **112**, 212002 (2014). arXiv:1312.5264 [hep-lat]
38. V. Lubicz et al. [ETM Collaboration], arXiv:1707.04529 [hep-lat]
39. B. Colquhoun, R. J. Dowdall, C. T. H. Davies, K. Hornbostel, G. P. Lepage, Phys. Rev. D **91**(7), 074514 (2015). arXiv:1408.5768 [hep-lat]